Phys Chem Minerals (2006) 33: 227–234
DOI 10.1007/s00269-006-0071-4

ORIGINAL PAPER

T. Kawazoe · E. Ohtani

Reaction between liquid iron and (Mg,Fe)SiO_3-perovskite and solubilities of Si and O in molten iron at 27 GPa

Received: 30 March 2005 / Accepted: 3 February 2006 / Published online: 9 March 2006

Abstract The Earth's core contains light elements and their identification is essential for our understanding of the thermal structure and convection in the core that drives the geodynamo and heat flow from the core to the mantle. Solubilities of Si and O in liquid iron coexisting with (Mg,Fe)SiO_3-perovskite, a major constituent of the lower mantle, were investigated at temperatures between 2,320 and 3,040 K at 27 GPa. It was observed that Si dissolved in the liquid iron up to 1.70 wt% at 3,040 K and O dissolved in the liquid iron up to 7.5 wt% at 2,800 K. It was also clearly seen that liquid iron reacts with (Mg,Fe)SiO_3-perovskite to form magnesiowüstite and it contains Si and O at 27 GPa and at 2,640 and 3,040 K. The amounts of Si and O in the liquid iron are 1.70 and 2.25 wt% at 3,040 K, respectively. The solubilities of Si and O in liquid iron coexisting with (Mg,Fe)SiO_3-perovskite have strong positive temperature dependency. Hence, they can be plausible candidates for the light elements in the core.

Keywords: (Mg,Fe)SiO_3-perovskite · Liquid iron · Silicon · Oxygen · Earth's core

Introduction

The Earth's core is supposed to contain light elements such as Si, O, and S based on the comparison of seismic observations with the equation of state of the core materials (e.g. Anderson and Isaak 2002), cosmochemial observations (e.g. Allegre et al. 2001), and the phase relations of the iron-light element systems at high pressures and temperatures (e.g. Hillgren et al. 2000). The light elements were dissolved in liquid iron to form the core (Hillgren et al. 2000). A terrestrial magma ocean is likely to have extended to the depth of lower mantle during the core formation stage (Ohtani et al. 1997; Righter et al. 1997; Li and Agee 2001b). Liquid iron that separated from the magma ocean ponded at the base, and segregated to form the core. The (Mg,Fe)SiO_3-perovskite (hereafter, Mg-perovskite), thought to be the most dominant mineral in the lower mantle, may have undergone reaction with liquid iron at the base of the deep magma ocean, which have provided Si and O as the light elements in the core. The dissolution of Si in liquid iron also makes it possible to explain its depletion in the primitive mantle compared with CI chondrite (McDonough and Sun 1995; Allegre et al. 2001) without enrichment in the lower mantle. Another important aspect of this reaction is that it may occur at the core–mantle boundary throughout the core formation stage. Results of previous studies on this reaction using a laser-heated diamond anvil cell (LH-DAC) (Knittle and Jeanloz 1989, 1991; Hillgren and Boehler 2000; Takafuji et al. 2005) are controversial. Knittle and Jeanloz (1989, 1991) reported that Mg-perovskite reacted with liquid iron to produce SiO_2-stishovite, $Fe_{0.9}O$-wüstite, and FeSi at 75 GPa and 3,700 K. On the other hand, Hillgren and Boehler (2000) performed the reaction experiments between liquid iron and Mg-perovskite up to 100 GPa and 3,300 K and found low solubilities of Si (<0.2 wt%) and O (<0.9 wt%) in the liquid iron and no reaction products such as SiO_2-stishovite, $Fe_{0.9}O$-wüstite, and FeSi reported by Knittle and Jeanloz (1989, 1991). Recently, Takafuji et al. (2005) investigated the reaction up to 97 GPa and 3,150 K and observed dissolution of Si (<3.1 wt%) and O (<5.3 wt%) in the liquid iron. In this study, equilibrium experiments between liquid iron and Mg-perovskite have been conducted with a Kawai-type multianvil apparatus at 27 GPa and up to 3,040 K in order to obtain more reliable results on this reaction, besides the solubilities of Si and O in the liquid iron. The present experiments have been conducted in the Fe–Mg–Si–O system to observe the reaction between liquid iron and Mg-perovskite based on a simple model system.

T. Kawazoe (✉) · E. Ohtani
Institute of Mineralogy, Petrology and Economic Geology,
Graduate School of Science, Tohoku University,
980-8578 Sendai, Japan
E-mail: kawazoe@ganko.tohoku.ac.jp
Tel.: +81-22-7956662
Fax: +81-22-7956675

Experimental methods

Experiments were performed using a Kawai-type multianvil apparatus at Tohoku University, using WC anvils with 2.0-mm truncated edges and a semi-sintered (Mg,Co)O pressure medium. Pure iron (99.99 wt% purity) rod was packed into a synthesized $MgSiO_3$ or $(Mg_{0.9},Fe_{0.1})SiO_3$ pyroxene capsule. In order to produce different oxygen fugacity (fO_2) conditions for the samples, we used $MgSiO_3$ and $(Mg_{0.9},Fe_{0.1})SiO_3$ pyroxene capsules and iron rods with differing volumes (Table 1). $MgSiO_3$ enstatite was synthesized from a mixture of MgO and SiO_2 reagents. The mixture was melted by shining the CO_2 laser and then quenched by turning the laser off. $(Mg_{0.9},Fe_{0.1})SiO_3$ pyroxene was synthesized from a mixture of reagent grade oxides of MgO, Fe_2O_3, and SiO_2 in a graphite capsule at 3 GPa and 1,673 K using a Kawai-type apparatus after heating the mixture in a CO_2–H_2 gas mix furnace at 1,527 K for 24 h with the oxygen fugacity approximately 2 log units below the fayalite–magnetite–quartz buffer.

The iron and pyroxene were heated at high temperature using a Re cylindrical heater and a $LaCrO_3$ thermal insulator system. Temperature was increased at a rate of 170 K/min to the desired value. The starting material (pyroxene) was transformed to Mg-perovskite before the temperature reached the melting point of iron during the temperature increase. This transformation was confirmed by the observation of Mg-perovskite in the sample, which was heated to 2,000 K at a rate of 170 K/min, similar to that mentioned above. Generated temperature was calibrated using the relation between input power to the heater and the melting temperature of Mg-perovskite (Zerr and Boehler 1993) and the eutectic temperature in the Fe–FeO system (Boehler 1993). This calibration is confirmed by a similar relationship between the power to the heater and the tem-

Table 1 Experimental conditions, compositions of run products (wt%), and quench products in liquid iron. All experiments have been conducted at 27 GPa

Run No.	83	111	110	102	86	84
Temperature (K)	3,040	2,960	2,800	2,800	2,640	2,320
Duration (min)	1	5	30	60	50	60
$\Delta\log fO_2$ (IW)	−1.70 (0.01)	−1.29 (0.25)*	−0.83 (0.27)*	−0.47 (0.27)*	−1.12 (0.02)	−0.31 (0.87)*
Starting material						
Silicate composition	$MgSiO_3$	$MgSiO_3$	$MgSiO_3$	$(Mg_{0.9},Fe_{0.1})SiO_3$	$MgSiO_3$	$MgSiO_3$
Fe volume (mm^3)	0.079	0.020	0.020	0.020	0.079	0.079
Mg-perovskite						
SiO_2	58.0 (0.5)	59.3 (0.5)	58.7 (0.8)	57.5 (0.6)	58.4 (0.7)	57.7 (0.4)
MgO	37.4 (0.4)	35.0 (0.3)	33.8 (0.6)	30.8 (0.7)	37.4 (0.7)	35.3 (0.6)
FeO	4.6 (0.4)	6.3 (0.3)	7.7 (0.3)	12.0 (0.7)	3.9 (0.6)	7.4 (0.7)
Total	100.0	100.6	100.2	100.3	99.7	100.4
n[a]	5	9	5	7	5	5
Magnesiowüstite						
SiO_2	0.5 (0.1)	–	–	–	0.9 (0.4)	–
MgO	79.1 (0.4)	–	–	–	60.8 (0.9)	–
FeO	20.6 (0.3)	–	–	–	38.5 (0.6)	–
Total	100.2	–	–	–	100.2	–
n[a]	6	–	–	–	6	–
Liquid iron						
Fe	96.5 (0.4)	97.2 (0.5)	93.5 (0.5)	92.4 (0.5)	97.5 (0.5)	99.6 (0.5)
Si	1.70 (0.02)	0.44 (0.07)	0.22 (0.03)	0.18 (0.03)	0.15 (0.02)	0.05 (0.01)
O	2.25 (0.01)	3.07 (0.04)	4.83 (0.06)	7.52 (0.10)	1.63 (0.02)	1.37 (0.02)
Total	100.5	100.7	98.5[b]	100.1	99.3[b]	101.1
n[a]	5	3	2	2	25	25
ϕ[c] (μm)	100	100	100	100	30	30
Quench products[d]	st, q-i, s-w	st, d-w, s-w	o-b, st, d-w, s-w	o-b, d-w, s-w	st, b, q-i, s-w	st, b, q-i, s-w
$K^{Mg\text{-}pv/mw}$ [e]	0.47 (0.06)	0.39 (0.11)[f]	0.26 (0.08)[f]	0.26 (0.08)[f]	0.17 (0.04)	0.06 (0.06)[f]

The numbers in parenthesis indicate standard deviation, σ. The standard deviation of Mg-perovskite and magnesiowüstite was calculated from multiple analyses at different positions. The standard deviation of liquid iron was based on five analyses performed at the same region. –, absence of magnesiowüstite in the run product

*$\Delta\log fO_2$ (IW) of runs #111, #110, #102, and #84 were estimated using interpolated and extrapolated $K^{Mg\text{-}pv/mw}$

[a]The number of analytical points

[b]Total is slightly lower than 100 wt% due to Re contamination from the heater

[c]Diameter of the electron beam applied for analyzing liquid iron

[d]*st* stishovite, *q-i* quenched crystal iron, *s-w* sub-micron wüstite, *d-w* dendritic wüstite, *o-b* oxide blob composed of FeO and Fe (see Fig. 7), *b* blob composed of FeO and SiO_2 (see Fig. 4b)

[e]Exchange partition coefficient $K^{Mg\text{-}pv/mw}$ between Mg-perovskite and magnesiowüstite, as defined in Eq. 1

[f]$K^{Mg\text{-}pv/mw}$ of runs #111, #110, #102, and #84 were interpolated or extrapolated from those of runs #83 and #86 quenched at 3,040 and 2,640 K, respectively

peratures monitored at the midpoint of the outer surface of the heater with a $W_{97}Re_3$–$W_{75}Re_{25}$ thermocouple in another experiment. Especially in run #83, quenched at 3,040 K and 27 GPa, Mg-perovskite was melted at the outer surface of the Mg-perovskite capsule, which was in contact with the Re heater. The result of the temperature calibration is shown in Fig. 1. The relation between the input power and temperature is comparable to that reported by Ito and Katsura (1992) using a similar cell assemblage used in this study. Uncertainties in temperatures estimated in this study were ±130 K, from the errors in melting temperatures used for the calibration. Ceramic components of the cell assemblage were dried at 850°C for several hours before the experiments. Generated pressure was calibrated using the phase transition pressure from ringwoodite to Mg-perovskite and periclase in Mg_2SiO_4 (Fei et al. 2004) and that from pyrope garnet to aluminous Mg-perovskite and corundum in $Mg_3Al_2Si_3O_{12}$ at 1,873 K (Hirose et al. 2001; Fei et al. 2004) based on the MgO pressure scale of Speziale et al. (2001) (Fig. 2). All experiments in the present study were conducted at 1,100 ton.

Quenched liquid iron was analyzed by an electron probe micro-analyzer (EPMA) in the wavelength dispersive mode (JEOL JXA-8200, 8800). A large electron beam diameter (100 or 30 μm) was applied for analyzing the liquid iron because it contained quench products and was not homogeneous. The chemical compositions of

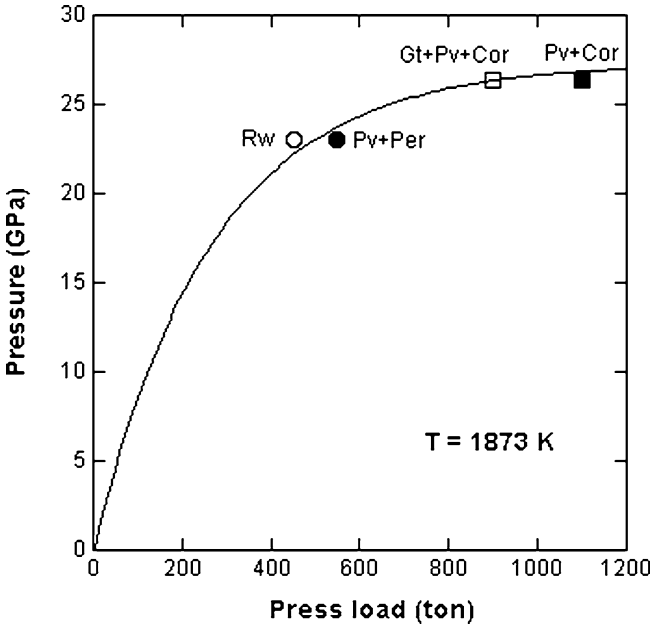

Fig. 2 Relation between press load and generated pressure at 1,873 K. Ringwoodite and an assemblage of Mg-perovskite and periclase were synthesized in Mg_2SiO_4 at 450 and 550 ton, respectively. We synthesized an assemblage of pyrope garnet, Mg-perovskite, and corundum and that of Mg-perovskite and corundum in $Mg_3Al_2Si_3O_{12}$ at 900 and 1,100 ton, respectively. *Rw* ringwoodite, *Pv* Mg-perovskite, *Per* periclase, *Gt* pyrope garnet, and *Cor* corundum

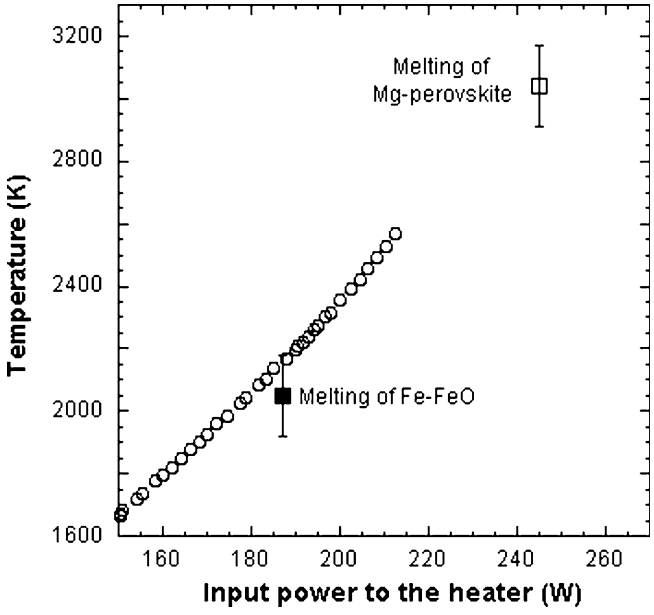

Fig. 1 Relationship between input power and temperature. Generated temperatures were calibrated using a relation between the input power to the heater and the melting temperature of Mg-perovskite (Zerr and Boehler 1993) and the eutectic temperature in the Fe–FeO system (Boehler 1993). The input power for the melting temperature of Mg-perovskite (3,040 ± 130 K; *open square*) and that for the eutectic temperature in the Fe–FeO system (2,050 ± 130 K; *filled square*) are shown. *Small circles* represent the input power and temperature monitored with the $W_{97}Re_3$–$W_{75}Re_{25}$ thermocouple in a separate run

Mg-perovskite and magnesiowüstite were analyzed with an EPMA in the energy dispersive mode (JEOL JSM-5410) and with a small electron beam (< 2 μm). Analytical errors of the compositions of liquid iron, Mg-perovskite, and magnesiowüstite listed in Table 1 were estimated from standard deviations of the multiple analyses. Crystal structures of the quench phases were identified using a micro-focus X-ray diffractometer (MAC Science, M18X-CE).

Results and discussion

Table 1 shows experimental conditions, compositions of run products, quench products in the liquid iron, and oxygen fugacity relative to the iron–wüstite buffer ($\Delta\log f O_2$ (IW)). We analyzed the compositions of Mg-perovskite and magnesiowüstite grains in contact with liquid iron in runs #83 and #86. These compositions did not show any significant variations between different analytical points since the standard deviations obtained from multiple analyses were smaller than 1.0 wt% for each component (Table 1). This suggests that these minerals were in local chemical equilibrium with each other. The run durations of the experiments at 2,960 and 3,040 K were relatively shorter than the other experiments in this study. However, the run durations are comparable to those of Ito and Katsura (1992). They reported that Mg-perovskite and magnesiowüstite were

in chemical equilibrium in the sample kept at 2,823 K and 24 GPa for 2.0 min using a similar Kawai-type multianvil apparatus. Thus, the experimental samples kept at 2,960 and 3,040 K appear to be in local chemical equilibrium due to the high temperature conditions.

Since fO_2 has a strong effect on solubilities of Si and O in liquid iron coexisting with the mantle minerals (Gessmann et al. 2001; Rubie et al. 2004), its evaluation in the sample is useful in separating the effect of temperature on the solubilities from that of fO_2. The iron–wüstite buffer is not calibrated at 27 GPa and 2,320 K, and therefore one cannot uniquely define the absolute value of fO_2 from the sample at the experimental conditions of the present study. However, the $\Delta\log fO_2$ (IW), useful in evaluating fO_2 from the sample under such conditions, can be calculated from the composition of the sample composed of iron-rich metal and oxide. The $\Delta\log fO_2$ (IW) was estimated using the following equation:

$$\Delta \log fO_2(\mathrm{IW}) = 2\log X_{\mathrm{FeO}}/X_{\mathrm{Fe}} \quad (1)$$

where X_{Fe} is the mole fraction of Fe in the run product from liquid iron and X_{FeO} is the mole fraction of FeO in magnesiowüstite (Gessmann et al. 2001). The calculated $\Delta\log fO_2$ (IW) varied from −0.40 to −1.70 depending on temperature, FeO content of pyroxene, and the encapsulated volume of metallic iron. In the runs where magnesiowüstite was not observed, we estimate the composition of magnesiowüstite using an exchange partition coefficient $K^{\mathrm{Mg\text{-}pv/mw}}$, which was obtained in this study. $K^{\mathrm{Mg\text{-}pv/mw}}$ is determined as

$$K^{\mathrm{Mg\text{ - }pv/mw}} = (X_{\mathrm{FeSiO_3}}X_{\mathrm{MgO}})/(X_{\mathrm{MgSiO_3}}X_{\mathrm{FeO}}) \quad (2)$$

where, $X_{\mathrm{FeSiO_3}}$, $X_{\mathrm{MgSiO_3}}$, X_{FeO} and X_{MgO} are the mol fraction of $FeSiO_3$ and $MgSiO_3$ in Mg-perovskite and FeO and MgO in magnesiowüstite, respectively. The $K^{\mathrm{Mg\text{-}pv/mw}}$ values determined from run #83 quenched at 3,040 K and run #86 quenched at 2,640 K were found to be 0.47 ± 0.06 and 0.17 ± 0.04, respectively. We see that the value of $K^{\mathrm{Mg\text{-}pv/mw}}$ increases with increasing temperature. This is in agreement with the results reported by Ito and Katsura (1992) and Katsura and Ito (1996). The $K^{\mathrm{Mg\text{-}pv/mw}}$ values obtained in this study were lower by a factor of ~0.3 compared to previous studies (Ito and Katsura 1992; Katsura and Ito 1996; Mao et al. 1997). This difference is probably due to the difference in ferric iron in Mg-perovskite due to the varying fO_2 conditions in the sample. Therefore, the $K^{\mathrm{Mg\text{-}pv/mw}}$ values of the runs quenched at 2,960, 2,800, and 2,320 K were estimated by interpolation or extrapolation from those runs quenched at 3,040 and 2,640 K in this study. We take the $K^{\mathrm{Mg\text{-}pv/mw}}$ value as an exponential function of the inverse of temperature considering $K^{\mathrm{Mg\text{-}pv/mw}} = \exp(-\Delta G^0/RT)$, where ΔG^0 is the standard state free energy change of an exchange reaction, T is the temperature in Kelvin, and R is the gas constant.

The run products from liquid iron were composed of α-Fe, FeO-wüstite, and SiO_2-stishovite, except for run #102 in which the product was composed of α-Fe and FeO-wüstite. We identified the SiO_2 phase as stishovite in the samples of runs #83, #110, and #111 using a micro-focus X-ray diffractometer. Existence of stishovite in the samples of runs #84 and #86 was estimated by their chemical compositions. Quench textures of liquid iron in runs #83, #86, #111, #110, and #102 are shown in Figs. 3, 4, 5, 6, and 7, respectively. They were found to be similar to that of melting experiments in the Fe–FeO system at 16 GPa (Ringwood and Hibberson 1990; Kato and Ringwood 1989), except for a precipitation of stishovite and blobs composed of SiO_2 and FeO, in this study. Quench products, except for stishovite, were systematically changed with increasing oxygen content in liquid iron. At lower oxygen content in the liquid iron, quench products were iron crystal, sub-micron wüstite and blobs composed of SiO_2 and FeO. At higher oxygen content they were found to be wüstite dendrite, sub-micron wüstite and blobs composed of FeO and Fe. The change in quench texture with increase of oxygen content can be seen in the sequence of Figs. 4b, 5a, 6, and 7. This is in agreement with the results of Ringwood and Hibberson (1990), and Kato and Ringwood (1989). The amount of stishovite increased with increasing temperature and decreasing oxygen content in liquid iron. These quench products are interpreted as dissolved in the liquid iron at high temperature and pressure and formed by precipitation from the liquid iron during rapid quenching (Ringwood and Hibberson 1990, 1991).

A reaction between the liquid iron and Mg-perovskite to form magnesiowüstite was clearly observed in runs #83 and #86 quenched at 3,040 and 2,640 K at 27 GPa, respectively; i.e., magnesiowüstite was distributed in the boundary between liquid iron and Mg-perovskite in these runs. Back-scattered electron images (BEI, hereafter) of these runs are shown in Figs. 3 and 4, respectively. We could not confirm the presence of magnesiowüstite in the other runs, although dissolution of Si in liquid iron was observed. This is probably due to very small amounts of magnesiowüstite in these runs as a result of the smaller volume of the liquid iron in runs #111, #110, and #102 besides the lower solubility of Si in the liquid iron in run #84, as compared to runs #83 and #86. The reaction between liquid iron and Mg-perovskite at 27 GPa and high temperature is described by the following equation:

$$\begin{aligned}&(\mathrm{Mg,Fe})\mathrm{SiO_3}(\mathrm{Mg\text{ - perovskite})}\\ &\quad = (\mathrm{Mg,Fe})\mathrm{O}(\mathrm{magnesiowüstite}) + \mathrm{Si}(\mathrm{in\ liquid\ iron})\\ &\qquad + 2\mathrm{O}(\mathrm{in\ liquid\ iron})\end{aligned} \quad (3)$$

This is the dissolution reaction of Si and O in liquid iron to form magnesiowüstite. Knittle and Jeanloz (1989, 1991) reported a reaction between liquid iron and Mg-perovskite up to 75 GPa and 3,700 K with LH-DAC and observed the formation of stishovite, wüstite, and Fe–Si with X-ray diffraction and dissolution of Si and O in the liquid iron using the EPMA

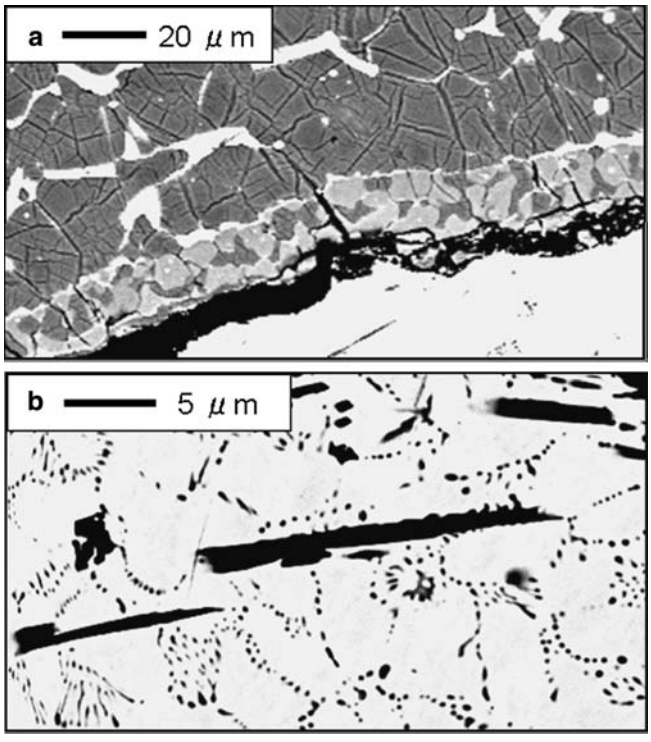

Fig. 3 BEI of run #83 quenched at 3,040 K and 27 GPa. **a** Mg-perovskite (*dark gray*) reacted with liquid iron (*white*) to form magnesiowüstite (*light gray*) at the boundary between Mg-perovskite and the liquid iron. We analyzed the compositions of Mg-perovskite grains in contact with liquid iron and magnesiowüstite. This reaction provides Si and O as "light elements" in liquid iron. A crack (*black zone*) between the liquid iron and a reaction zone was formed during decompression. **b** Needle-like stishovite (*black*) was grown over iron quench crystals (*white*) and many sub-micron wüstite (*gray area*) were formed between the iron quench crystals. Si and O contents in the liquid iron were found to be 1.70 and 2.3 wt%, respectively

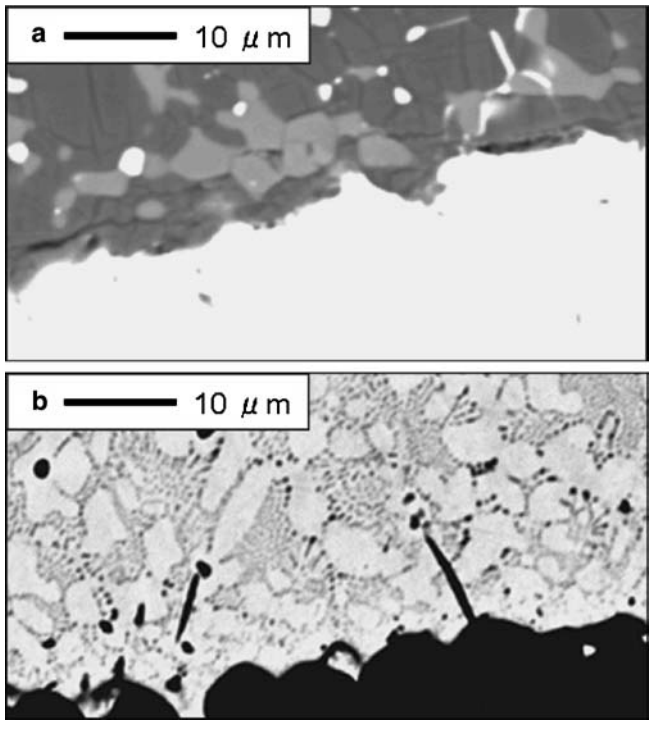

Fig. 4 BEI of run #86 quenched at 2,640 K and 27 GPa. **a** The reaction between Mg-perovskite (*dark gray*) and liquid iron (*white*) to form magnesiowüstite (*light gray*) was clearly observed at the boundary region between Mg-perovskite and the liquid iron. **b** Stishovite (*black, needle-like*) was observed only at the outer part of liquid iron in contact with Mg-perovskite (*black, lower part*). Blobs composed of SiO_2 and FeO (*black, spherule*), iron quench crystal (*white*), and sub-micron wüstite (*gray area*) are also seen in the liquid iron

analysis. We interpret that stishovite, wüstite, and Fe–Si alloy, as reported by them were crystallized from liquid iron containing Si and O. Recently, Takafuji et al. (2005) investigated the reaction between liquid iron and Mg-perovskite up to 97 GPa and 3,150 K using LH-DAC. They reported that the quenched liquid iron was composed of fine-grained aggregates of quench crystals of iron, wüstite, and stishovite. These quench products are in good agreement with those observed in this study. However, they could not observe any grains of such quench crystals from the bright field image obtained using a transmission electron microscope. In this study, iron quench crystals, wüstite and stishovite were observed by scanning electron microscope. Differences in the quench textures between those of Takafuji et al. (2005) and this study may be due to the difference in the speed of quenching of the samples using LH-DAC and the Kawai-type multianvil apparatus.

The dependence of the solubilities of Si and O in liquid iron on temperature and fO_2 is important in order to ascertain the amount of Si and O that the liquid iron could contain during the core formation stage. The contents of Si and O in the liquid iron coexisting with Mg-perovskite at 27 GPa and high temperatures are shown in Fig. 8. We also calculated the dependence of the solubilities of Si and O on fO_2 at 27 GPa and varying temperatures (2,320, 2,400, 2,800, and 3,040 K) and showed in the same figure. The dissolution reaction of Si and O in the present experiments may be expressed as follows: $SiO_2(\text{in Mg - perovskite}) \rightarrow Si(\text{in metal}) + 2O(\text{in metal})$, and $FeO(\text{in magnesiowüstite}) \rightarrow Fe(\text{in metal}) + O(\text{in metal})$ (O'Neill et al. 1998; Gessmann et al. 2001). The solubilities of Si and O in the liquid iron can be related to the temperature and fO_2 using the relationship between free energy change ΔG^0, equilibrium constant K, and thermodynamic parameters for each reactions ($\Delta G^0 = -RT\ln K = \Delta H^0 - T\Delta S^0 + P\Delta V^0$, where P is the pressure and ΔH^0, ΔS^0, and ΔV^0 are the changes of enthalpy, entropy, and volume, respectively). These reactions give rise to the following thermodynamic equations (O'Neill et al. 1998; Gessmann et al. 2001; Rubie et al. 2004)

$$\ln X_{Si} = -2.30\Delta\log fO_2(\text{IW}) + a/R + b/RT \quad (4)$$

and

$$\ln X_O = 1.15\Delta\log fO_2(\text{IW}) + c/R + d/RT \quad (5)$$

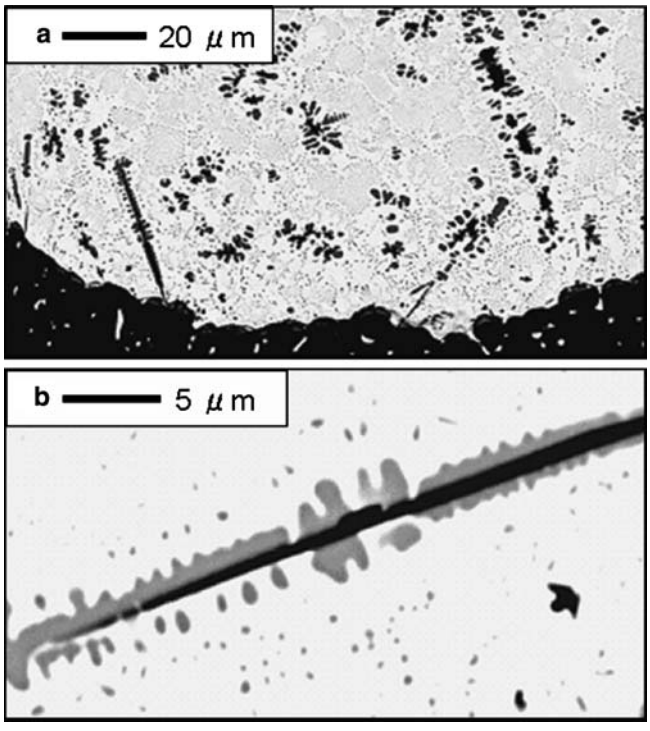

Fig. 5 BEI of run #111 quenched at 2,960 K and 27 GPa. **a** Needle-like stishovite, dendritic wüstite (*black*) and sub-micron wüstite (*gray area*) were precipitated in the liquid iron. Lower black part is Mg-perovskite. **b** Wüstite (*gray*) grew around needle-like stishovite (*black*)

where X_{Si} and X_O are the mole fractions of Si and O in liquid iron, respectively, and a, b, c, and d are constants. We determined these constants in Eqs. 4 and 5 by fitting the six compositional data of each element (Table 1) using the method of least squares. As a result, the constants are deduced as $a = -21.8$ (± 29.2), $b = -119$ (± 83)$\times 10^3$, $c = 45.9$ (± 18.3), and $d = -155$ (± 52)$\times 10^3$. We thus find that the solubilities of Si and O increases significantly with increasing temperature at constant fO_2 and pressure, and that the solubility of Si decreases and

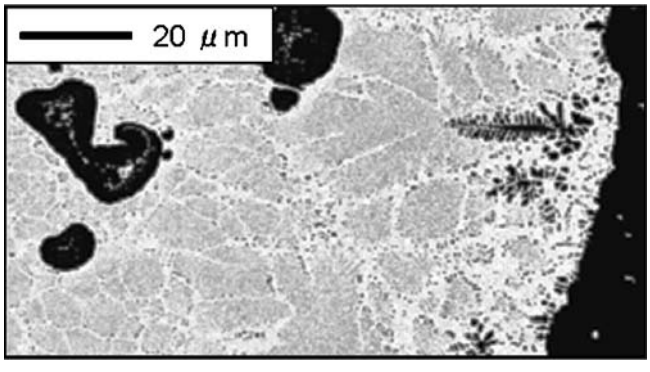

Fig. 6 BEI of run #110 quenched at 2,800 K and 27 GPa. Ionic liquid (*black, spherule*) was observed at the central region of liquid iron. Dendritic wüstite was observed at the outer region in contact with Mg-perovskite (*black, right-hand side*). Sub-micron wüstite (*gray area*) precipitated homogeneously

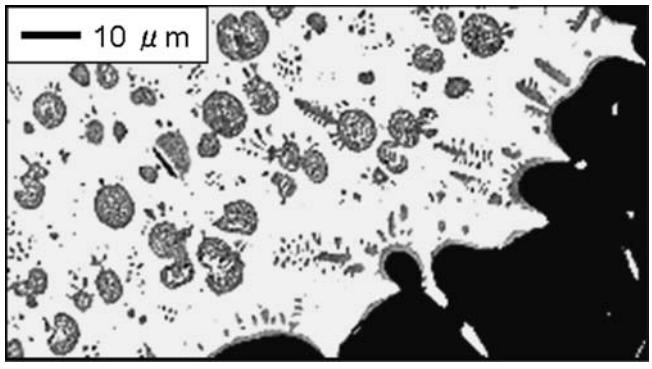

Fig. 7 BEI of run #102 quenched at 2,800 K and 27 GPa. Ionic blob (*gray, spherule*) and dendritic wüstite (*gray*) were observed homogeneously in the liquid iron. Black grains were found to be Mg-perovskite. Si and O contents in the liquid iron were 0.18 and 7.52 wt%, respectively

that of O increases with increasing fO_2 at constant temperature and pressure, as shown in Fig. 8. Their positive temperature dependence is consistent with those observed in liquid iron in equilibrium with the liquid silicate, magnesiowüstite and/or olivine polymorphs at high pressures and temperatures (Li and Agee 2001a; Gessmann et al. 2001; Rubie et al. 2004).

During the core formation stage, liquid iron descended into the magma ocean, then ponded at its bottom and subsequently descended through the solid mantle composed of Mg-perovskite and magnesiowüstite to the center of the proto-Earth. As the depth of the magma ocean increased, pressure and temperature at the bottom of the magma ocean increased along the mantle solidus (Zerr et al. 1998). According to recent studies on partitioning of siderophile elements between liquid iron and magma or magnesiowüstite (e.g. Gessmann and Rubie 2000; Li and Agee 2001b; Bouhifd and Jephcoat 2003), the magma ocean could have been extended to the upper part of the lower mantle and $\Delta\log fO_2$ (IW) of the magma ocean was considered to be in the range between -2.5 and -2.1 (Gessmann and Rubie 2000). If the magma ocean had extended to a pressure of level of 27 GPa, then the temperature at the bottom of the magma ocean can be estimated to be between 2,400 and 2,800 K, based on the solidus temperature of pyrolite (Zerr et al. 1998). Equations 4 and 5 indicate that the Si solubility in the liquid iron is more than 1.2 wt% and that of O, between 0.2 and 0.9 wt% at these fO_2 and temperature values, as can be seen in Fig. 8. Therefore, considerable amounts of Si and O can be dissolved in the liquid iron ponded at the bottom of the magma ocean when it had extended to a pressure of 27 GPa. Rubie et al. (2004) suggested that O solubility in the liquid iron could increase with increasing depth of the magma ocean beyond 27 GPa because of the positive dependence of the solubility of O on temperature being larger than the negative dependence on pressure in this region. On the other hand, Takafuji et al. (2005) have reported the positive pressure dependence of the solubilities of O

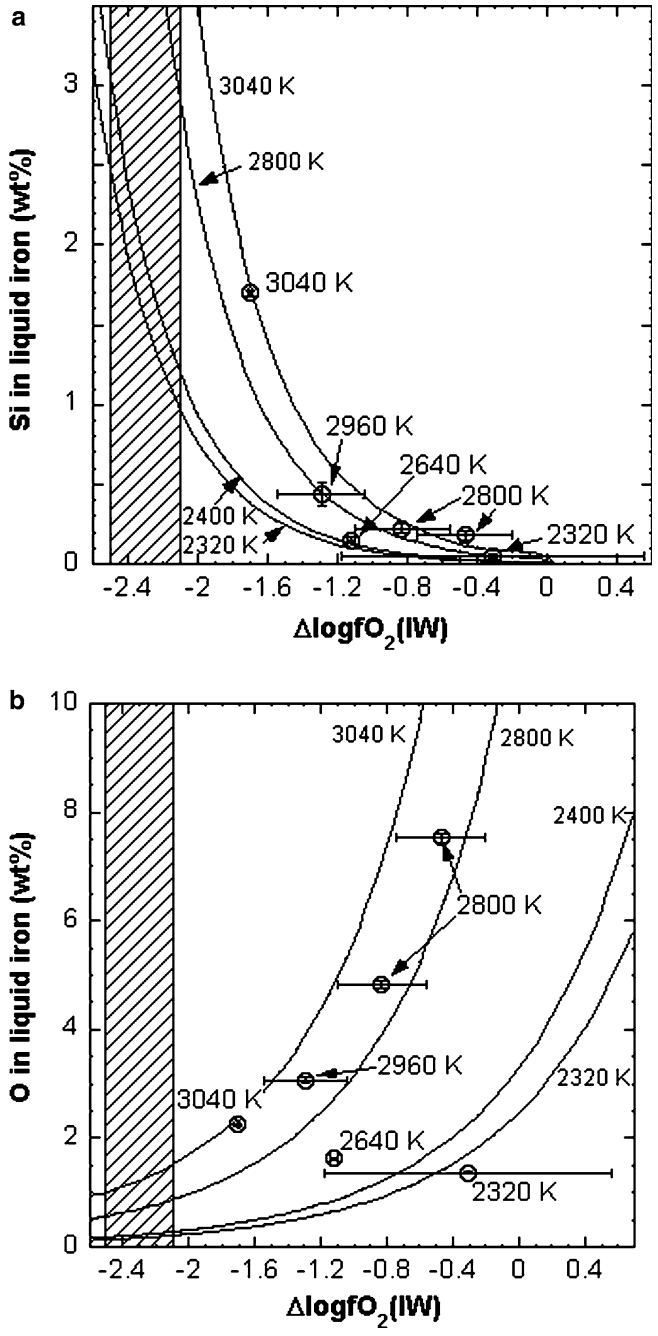

Fig. 8 The oxygen fugacity dependence of Si (**a**) and O (**b**) contents in liquid iron coexisting with Mg-perovskite at 27 GPa and high temperatures. *Open circles* represent the Si and O contents in the liquid iron. The *solid curves* show the solubilities of Si and O at 3,040, 2,800, 2,400, and 2,320 K as deduced from Eqs. 4 and 5. Temperature at the bottom of the magma ocean at 27 GPa, which was one of the conditions of the experiments performed in this study, was found to be in the range between 2,400 and 2,800 K (Zerr et al. 1998). $\Delta\log fO_2$ (IW) in the magma ocean was estimated to be in the range between −2.5 and −2.1 by Gessmann and Rubie (2000), and are shown as the hatched areas in the figures

in liquid iron coexisting with Mg-perovskite. Therefore, the above estimate of O content could be the lower bound. The liquid iron could contain several wt% of Si when the magma ocean extended to pressures greater than 27 GPa, taking into account the positive dependence on temperature, found in this study, and pressure (Takafuji et al. 2005) of the solubility of Si in the liquid iron coexisting with Mg-perovskite. Thus Si and O, explaining the density deficit of the present core (Anderson and Isaak 2002; Hirao et al. 2004), could have been transported by the liquid iron into the center of the Earth during the core formation stage.

Acknowledgments We thank Y. Ito and Y. Sato (nano-technical laboratory) for analyzing the run products with EPMA. We are grateful to two anonymous reviewers for helpful comments. This work was financially supported by the grant-in-aid of the Scientific Research (S) of the Ministry of Education, Culture, Science, Sport, and Technology of the Japanese Government (no. 14102009) to E.O., and conducted as a part of the twenty-first century center-of-excellence program of Tohoku University "Advanced Science and Technology Center for the Dynamic Earth".

References

Allegre C, Manhes G, Lewin E (2001) Chemical composition of the Earth and the volatility control on planetary genetics. Earth Planet Sci Lett 185:49–69

Anderson OL, Isaak DG (2002) Another look at the core density deficit of Earth's outer core. Phys Earth Planet Inter 131:19–27

Boehler R (1993) Temperatures in the Earth's core from melting-point measurements of iron at high static pressures. Nature 363:534–536

Bouhifd MA, Jephcoat AP (2003) The effect of pressure on partitioning of Ni and Co between silicate and iron-rich metal liquids: a diamond-anvil cell study. Earth Planet Sci Lett 209:245–255

Fei Y, Van Orman J, Li J, van Westrenen W, Sanloup C, Minarik W, Hirose K, Komabayashi T, Walter M, Funakoshi K (2004) Experimentally determined postspinel transformation boundary in Mg_2SiO_4 using MgO as an internal pressure standard and its geophysical implications. J Geophys Res 109:B02305

Gessmann CK, Rubie DC (2000) The origin of the depletions of V, Cr and Mn in the mantles of the Earth and Moon. Earth Planet Sci Lett 184:95–107

Gessmann CK, Wood BJ, Rubie DC, Kilburn MR (2001) Solubility of silicon in liquid metal at high pressure: implications for the composition of the Earth's core. Earth Planet Sci Lett 184:367–376

Hillgren VJ, Boehler R (2000). High pressure geochemistry in the diamond cell to 100 GPa and 3300 K. In: Manghnani MH, Nellis WJ, Nicol MF (eds) Proceedings of AIRAPT-17. Universities Press, Hyderabad, pp 609–611

Hillgren VJ, Gessmann CK, Li J (2000) An experimental perspective on the light element in the Earth's core. In: Canup RM, Righter K (eds) Origin of the Earth and Moon. Arizona University Press, Tucson, pp 245–263

Hirao N, Ohtani E, Kondo T, Kikegawa T (2004) Equation of state of iron–silicon alloys to megabar pressure. Phys Chem Minerals 31:329–336

Hirose K, Fei Y, Ono S, Yagi T, Funakoshi K (2001) In situ measurements of the phase transition boundary in $Mg_3Al_2Si_3O_{12}$: implications for the nature of the seismic discontinuities in the Earth's mantle. Earth Planet Sci Lett 184:567–573

Ito E, Katsura T (1992) Melting of ferromagnesian silicates under the lower mantle conditions. In: Syono Y, Manghnani MH (eds) High-pressure research: application to Earth and planetary sciences. Terra Scientific/American Geophysical Union, Tokyo/ Washington, DC, pp 315–322

Kato T, Ringwood AE (1989) Melting relationships in the system Fe–FeO at high pressures: implications for the composition and formation of the Earth's core. Phys Chem Minerals 16:524–538

Katsura T, Ito E (1996) Determination of Fe–Mg partitioning between perovskite and magnesiowüstite. Geophys Res Lett 23:2005–2008

Knittle E, Jeanloz R (1989) Simulating the core–mantle boundary: an experimental study of high-pressure reactions between silicates and liquid iron. Geophys Res Lett 16:609–612

Knittle E, Jeanloz R (1991) Earth's core–mantle boundary: results of experiments at high pressures and temperatures. Science 251:1438–1443

Li J, Agee CB (2001a) Element partitioning constraints on the light element composition of the Earth's core. Geophys Res Lett 28:81–84

Li J, Agee CB (2001b) The effect of pressure, temperature, oxygen fugacity and composition on partitioning of nickel and cobalt between liquid Fe–Ni–S alloy and liquid silicates: implications for the Earth's core formation. Geochim Cosmochim Acta 65:1821–1832

Mao H, Shen G, Hemley RJ (1997) Multivariable dependence of Fe–Mg partitioning in the lower mantle. Science 278:2098–2100

McDonough WF, Sun SS (1995) The composition of the Earth. Chem Geol 120:223–253

Ohtani E, Yurimoto H, Seto S (1997) Element partitioning between metallic liquid, silicate liquid, and lower mantle minerals: implication for core formation of the Earth. Phys Earth Planet Inter 100:97–114

O'Neill HS, Canil D, Rubie DC (1998) Oxide-metal equilibria to 2500°C and 25 GPa: implications for core formation and the light component in the Earth's core. J Geophys Res 103:12239–12260

Righter K, Drake MJ, Yaxley G (1997) Prediction of siderophile element metal/silicate partition coefficients to 20 GPa and 2800°C: the effects of pressure, temperature, oxygen fugacity, and silicate and metallic melt compositions. Phys Earth Planet Inter 100:115–134

Ringwood AE, Hibberson W (1990) The system Fe–FeO revisited. Phys Chem Minerals 17:313–319

Ringwood AE, Hibberson W (1991) Solubilities of mantle oxides in molten iron at high pressures and temperatures: implications for the composition and formation of Earth's core. Earth Planet Sci Lett 102:235–251

Rubie DC, Gessmann CK, Frost DJ (2004) Partitioning of oxygen during core formation on the Earth and Mars. Nature 429:58–61

Speziale S, Zha C, Duffy TS, Hemley RJ, Mao HK (2001) Quasi-hydrostatic compression of magnesium oxide to 52 GPa: implications for the pressure–volume–temperature equation of state. J Geophys Res 106:515–528

Takafuji N, Hirose K, Mitome M, Bando Y (2005) Solubilities of O and Si in liquid iron in equilibrium with $(Mg,Fe)SiO_3$ perovskite and the light elements in the core. Geophys Res Lett 32:L06313

Zerr A, Boehler R (1993) Melting of $(Mg,Fe)SiO_3$-perovskite to 625 kilobars: indication of a high melting temperature in the lower mantle. Science 262:553–555

Zerr A, Diegeler A, Boehler R (1998) Solidus of earth's deep mantle. Science 281:243–246